A Weighted Average Phase Velocity Inversion Model for Depth-Resolved Elasticity Evaluation in Human Skin In-Vivo

Zhou, Kanheng; Feng, Kairui; Li, Chunhui; Huang, Zhihong

Published in:
IEEE Transactions on Biomedical Engineering

DOI:
10.1109/TBME.2020.3045133

Publication date:
2021

Document Version
Peer reviewed version

Zhou, K, Feng, K, Li, C & Huang, Z 2020, 'A Weighted Average Phase Velocity Inversion Model for Depth-Resolved Elasticity Evaluation in Human Skin In-Vivo', IEEE Transactions on Biomedical Engineering. https://doi.org/10.1109/TBME.2020.3045133

SUPPLEMENTARY DOCUMENT

The weighting function in the forward model was derived from the numerical solutions of the wave equations describing the propagation of surface acoustic wave (SAW) in two-layer materials, and then extended to the layered materials with N layers ($N>2$).

A. Numerical simulations of SAW in two-layer materials

1) Physical model definition

In a spatially infinite, linear elastic, isotropic, two-layer material, as shown in Fig. S1(a), the equations of motion for SAW (Rayleigh wave) propagation in a 2D plane (x-z plane) can be expressed as:

$$\rho\frac{\partial^2\boldsymbol{u}}{\partial t^2}=(\Lambda+M)\nabla\nabla\cdot\boldsymbol{u}+M\nabla^2\boldsymbol{u} \tag{S1}$$

with the following mechanical boundary conditions on stress σ:

$$\begin{cases}\sigma_{zx}\big|_{z=0}=0\\ \sigma_{zz}\big|_{z=0}=0\\ \sigma_{zx}^{(1)}\big|_{z=h}=\sigma_{zx}^{(2)}\big|_{z=h}\\ \sigma_{zz}^{(1)}\big|_{z=h}=\sigma_{zz}^{(2)}\big|_{z=h}\end{cases} \tag{S2}$$

where $\boldsymbol{u}$ is the displacement vector field of the elastic waves in x-z plane, Λ and M are Lamé constants of the material, ρ is the mass density of the material, ∇ is the gradient operator, $\nabla\cdot$ is the divergence operator and ∇^2 is the Laplacian.

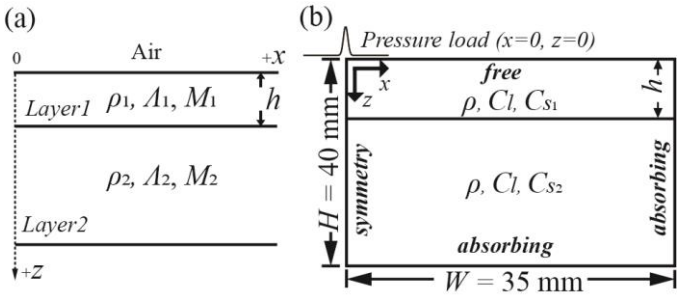

Fig. S1. (a) Illustration of a spatially infinite, linear elastic, isotropic, two-layer material for SAW propagation. (b) Geometry and boundary conditions for numerical simulation of SAW propagation in two-layer materials.

2) Numerical simulation setups

OnScale (OnScale 1.30.6.0, Redwood City, CA, USA) was employed to solve the elastic wave equations (S1) and (S2) numerically in this study. The geometry for the numerical simulation, as shown in Fig. S1(b), consists of two linear elastic regions separated by a horizontal plane located at depth z=h. Five layer thickness (0.1 mm, 0.3 mm, 0.6 mm, 1.0 mm and 2.0 mm) that covers the typical layer thickness of skin were assigned in the simulations. The top-layer shear wave velocity was set as 8 m/s, while the shear wave velocity in the bottom layer was looped from 1 m/s to 7 m/s with an increment of 1 m/s during the simulation to explore the behaviour of SAW at various top-bottom-velocity ratios for the purpose of achieving a robust forward model. The material density ρ (1000 kg/m^3) and longitudinal wave velocity (158.2 m/s [36]) were kept uniform across the domain.

To induce the SAW, a spatially and temporally varying pressure load was applied along the top boundary of the geometry. The spatial profile of the pressure load was defined by a super-Gaussian function [36]:

$$P(x)=a\cdot e^{-4\log 2\left(\frac{x}{d}\right)^2} \tag{S3}$$

where a is the normalised amplitude 1 and the d represents the contact length between the actuator head and sample, e.g., ~0.5 mm in our case. The temporal push profile of the load was obtained by directly measuring the vibration from the actuator head under a 0 ~ 25 kHz chirp driving signal.

To obtain accurate simulation results, a rectangular mesh grid with 40 elements per wavelength were employed. The running time for each simulation was set to be 5.5 ms, equivalent to that of one OCT M-scan. The bottom and right boundaries were set to be absorbing to minimize the wave reflections on these edges. The particle vibration velocity field in the vertical direction was output for post-processing.

3) Simulation data processing

All 35 simulation datasets (the spatial-temporal slice at the top surface) were processed by a two-dimensional fast Fourier transform (2D-FFT) analysis [7] for phase velocity dispersion curve reconstruction over a frequency range of 0 ~ 25 kHz. These frequency-dependent phase velocity dispersion curves $C_R(f)$ were then converted to wavelength domain, normalised to the top-layer thickness, e.g., $C_R(h/\lambda)$, and averaged for forward model derivation.

B. Derivation of the weighting function in layered materials

1) Two-layer material

Based on the hypothesis in [9], in C_R-$\frac{h}{\lambda}$ domain, the phase velocities in a two-layer material can be written as:

$$C_R\left(\frac{h}{\lambda}\right)=\left(\frac{0.87+1.12\upsilon}{1+\upsilon}\right)\left(W_1\left(\frac{h}{\lambda}\right)\cdot C_{S(1)}+W_2\left(\frac{h}{\lambda}\right)\cdot C_{S(2)}\right) \tag{S4}$$

where υ is the Poisson's ratio (assumed to be 0.5 in this study), $C_{S(1)}$ and $C_{S(2)}$ are the shear wave velocity of the first and second layer, W_1 and W_2 represents the weighting factor of the first and second layer, and $W_1+W_2=1$. Therefore, the wavelength-dependent top-layer weighting factor can be calculated as:

$$W_1\left(\frac{h}{\lambda}\right)=\frac{\left(\frac{1+\upsilon}{0.87+1.12\upsilon}\right)C_R\left(\frac{h}{\lambda}\right)-C_{S(2)}}{C_{S(1)}-C_{S(2)}} \tag{S5}$$

Based on (S5), top-layer weighting factors for all configurations were calculated and averaged, as shown in Fig. S2. For $\lambda > h$, the contribution of the shear wave velocity in the top layer decreases as the wavelength increases. In contrast, for $\lambda \le h$, the top layer weight gradually approaches and stabilizes at 1. A piecewise function was then found to approximate the measured wavelength-dependent top-layer weighting factors:

$$\begin{cases} W_1(\frac{h}{\lambda}) = Ae^{B\frac{h}{\lambda}} + Ce^{D\frac{h}{\lambda}} + Ee^{F\frac{h}{\lambda}} & (\frac{h}{\lambda} \le 1.425) \\ W_1 = 1 & (\frac{h}{\lambda} > 1.425) \end{cases} \quad \text{(S6)}$$

where parameters A to F equal to -6, -3.329, 5, -3.766, 1 and 0.02005, separately. The breakpoint (h/λ = 1.425) of this piecewise function was determined by the first point at which the top-layer weighting factor approaches 1. It can be seen the predicted top-layer weighting factor curve, plotted as a red dashed line in Fig. S2(a), matches reasonably well with the average one.

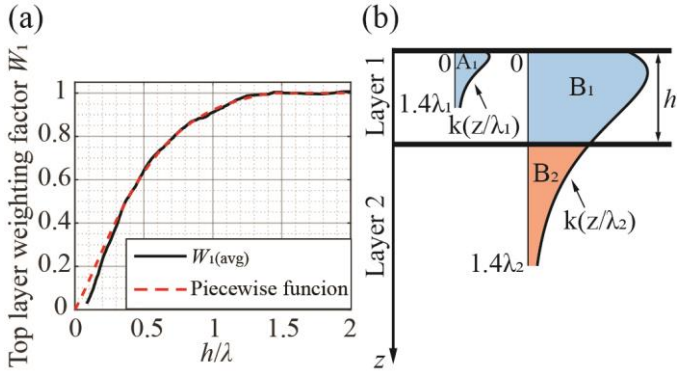

Fig. S2. (a) Averaged top-layer weighting factor $W_{1(avg)}$ (black solid line) with its piecewise function approximation (red dashed line). (b) Illustration of wavelength-dependent weighting factor calculation using (S7) in a two-layer material.

To extend the weighting factor approximation function (S6) to multi-layered materials, we rewrote this function as the integral of depth z:

$$\begin{cases} W_1(\lambda) = \dfrac{\int_0^h k(\frac{z}{\lambda})dz}{\int_0^{1.425\lambda} k(\frac{z}{\lambda})dz} = 1 & (\lambda < \dfrac{h}{1.425}) \\ W_1(\lambda) = \dfrac{\int_0^h k(\frac{z}{\lambda})dz}{\int_0^{1.425\lambda} k(\frac{z}{\lambda})dz} & (\lambda \ge \dfrac{h}{1.425}) \end{cases} \quad \text{(S7)}$$

where the integral kernel $k(z/\lambda)$ is the first order derivative of (S6) with respect to (z/λ) (h/λ in (S6)):

$$\begin{cases} k(\frac{z}{\lambda}) = ABe^{B\frac{z}{\lambda}} + CDe^{D\frac{z}{\lambda}} + EFe^{F\frac{z}{\lambda}} & (\frac{z}{\lambda} \le 1.425) \\ k(\frac{z}{\lambda}) = 0 & (\frac{z}{\lambda} > 1.425) \end{cases} \quad \text{(S8)}$$

An illustration for wavelength-dependent weighting factor calculation using (S7) in a two-layer material is shown in Fig. S2(b). In the case of h>1.425λ_1, the integral kernel only exists in the first layer for the entire integration range, therefore, $W_1(\lambda_1)$ that is the ratio of areas under the integral kernel equals to 1. The corresponding bottom-layer weighting factor $W_2(\lambda_1)$ is thus calculated to be 0 as the sum of all weighting factors equals to 1. While in the case of h>1.425λ_2, the integral kernel cross both layers. Then, there are two areas under the kernel. The area B_1 is the area within the first layer bounded by the kernel from the surface (z=0) to the two-layer interface (z=h). The area B_2 is the area in the second layer bounded by the kernel from the two-layer interface (z=h) to 1.425λ_2. In this case, $W_1(\lambda_2)$ that is the ratio of the area within layer 1 to the total area equals to $B_1/(B_1+B_2)$. Consequently, the bottom-layer weighting factor $W_2(\lambda_2)$ that is the ratio of the area within layer 2 to the total area equals to $B_2/(B_1+B_2)$, which could also be rewritten in the integral form as:

$$W_2(\lambda_2) = \frac{\int_h^{1.425\lambda_2} k(\frac{z}{\lambda})dz}{\int_0^{1.425\lambda_2} k(\frac{z}{\lambda})dz} \quad \text{(S9)}$$

2) Mult-layered material

Based on (S7) and (S9), the weighting factor of each layer at any wavelength $W_i(\lambda)$ in a multi-layered material can be expressed as:

$$W_i(\lambda) = \frac{\int_{Z_{i-1}}^{Z_i} k(\frac{z}{\lambda})dz}{\int_0^{1.425\lambda} k(\frac{z}{\lambda})dz} \quad \text{(S10)}$$

where Z_{i-1} represents the depth from the surface to the top of the ith layer, and Z_i denotes the depth from the surface to the bottom of the ith layer.

C. Comparison between the integral kernel function and the SAW axial displacement profiles

Fig. S3. illustrates the comparison between the integral kernel function and normalised SAW axial displacement profiles of different configurations. As the depth increases, the normalised amplitude of SAW axial displacement increases first, reaches its maximum of ~1.2 (~20% higher than the amplitude at the surface) at a depth of 10% ~20% wavelength, and then quickly decays to ~ 0 ~ 0.2 at 130% wavelength. The integral kernel, which was generated from the average of all cases, matches the trend of these SAW axial displacement profiles well, thus it is able to provide a reasonable approximation for a variety of layer thickness and shear wave velocity configurations.

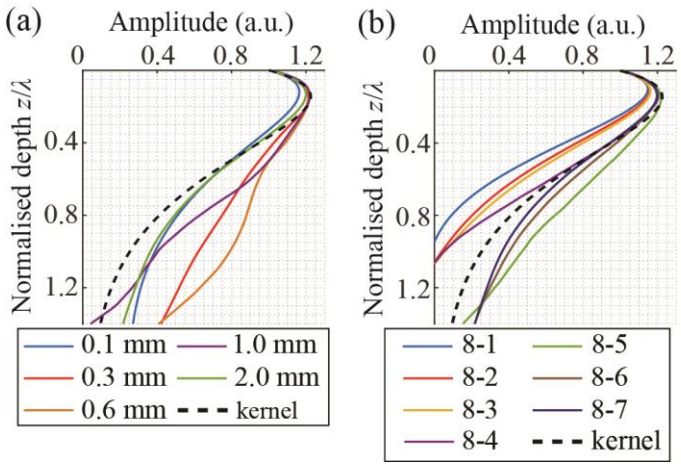

Fig. S3. (a) Comparison between normalised SAW axial displacement profiles of different layer thickness (solid colour lines) and the integral kernel function (black dashed line). (b) Comparison between normalised SAW axial displacement profiles of various shear wave velocity configurations (solid colour lines) and the integral kernel function (black dashed line). For all displacement profiles, the axial displacement was normalised to the displacement at surface (z=0), and the depth was normalised to the SAW wavelength.